stellarator news

Published by Fusion Energy Division, Oak Ridge National Laboratory
Building 9201-2 P.O. Box 2009 Oak Ridge, TN 37831-8071, USA

Editor: James A. Rome Issue 55 January 1998
E-Mail: jar@ornl.gov Phone (423) 574-1306 Fax: (423) 241-6211
On the Web at *http://www.ornl.gov/fed/stelnews*

TJ-II first plasma

On Tuesday, December 16, 1997, at 18:05, the first plasma was produced in the TJ-II flexible Heliac at CIEMAT in Madrid, Spain. The experiment was performed by launching a 300-kW microwave beam at 53.2 GHz into TJ-II, operating at its nominal field of 1 T. The picture in Fig. 1 shows the plasma's characteristic bean shape. Closed and nested magnetic surfaces were previously measured using electron-beam mapping techniques, proving the construction quality of this sophisticated, scientifically and technologically challenging stellarator.

The experimental life of TJ-II starts with a 1-MW electron cyclotron resonance heating (ECRH) system that will be immediately followed by two neutral beam injection (NBI) lines of 1.5 MW each (1999). A total of 5 MW of additional heating is projected for the experiment.

Carlos Alejaldre, Head of Research Unit
Asociacion EURATOM-CIEMAT para Fusion
Av. Complutense 22, 28040 Madrid, Spain
Phone: +34-1-346.6159, +34-1-346.6153
Fax: +34-1-346.6124
E-mail: Carlos.Alejaldre@ciemat.es
URL: http://www-fusion.ciemat.es/

Fig. 1. TJ-II first plasma.

In this issue . . .

Soft X-ray tomography of plasma equilibria and MHD modes at Wendelstein 7-AS

Introduction

The use of soft X radiation is widely used for detection of MHD activity in the plasmas of fusion devices [1]. It is also possible to use soft X radiation to measure the poloidal cross section of the flux surfaces if they are assumed to have constant emissivity in this part of the spectrum. In the case of the stellarator Wendelstein 7-AS (W7-AS), the specific magnetic configuration is the result of an optimization procedure [2]. However, compared with the axisymmetric tokamak configuration, stellarator flux surfaces have no toroidal symmetry and are characteristically shaped in a poloidal plane. Tomographic reconstruction of these typically formed surfaces and detection of MHD activity without making additional assumptions about the topology, requires a tomographic system with enhanced poloidal and radial resolution. This has been achieved with a system that has a high number of measurement channels and a well-balanced distribution over the poloidal plane.

The complete tomographic system includes both hardware and software (i.e., the reconstruction algorithm and further data processing methods). After describing this system, we show some applications to measurements of equilibrium flux contours and MHD activity as seen in W7-AS.

The 10-camera tomographic system at W7-AS

Figure 1 shows an overview of the hardware of the tomographic system and the idealized lines of sight of the X-ray detectors. To overcome the technical restriction of access from the inboard side of the torus, a small detector system was installed inside the vacuum vessel. The lines of sight are arranged in 10 fan-like groups, each group corresponding to a pinhole camera that is built up with 32 detectors (Si diode array on one chip) and a curved 6-mm Be filter. This gives an overall number of 320 channels, resulting in good spatial resolution that is comparable with the separation between neighboring lines (about 1 cm). Data acquisition is performed with a sampling rate of up to 200 kHz and a typical time window of about 20 ms at high sampling rates (limited by a maximum total data amount of 8 MByte per shot).

Three different algorithms for the 10-camera tomography and additional techniques are used to extract the relevant physical data (see Table 1). A choice can be made among algorithms using first-order regularization [3], which try to avoid steep gradients, a minimum Fisher information regularization scheme [4], and the maximum entropy [5, 6] solution. The tomographic result is defined by the mini-

Table 1. Tomography algorithms

First-order regularization:
$\Lambda_{\mathrm{LinReg}} = \frac{1}{2}\chi^2 + \alpha_R R\,, \qquad R = \int \lVert\nabla\rho\rVert^2$
Minimum Fisher information:
$\Lambda_{\mathrm{MinFisher}} = \frac{1}{2}\chi^2 + \alpha_R I_F\,, \qquad I_F = \int \frac{\rho'(x)^2}{\rho(x)}dx$
Maximum entropy:
$\Lambda_{\mathrm{MaxEnt}} = \frac{1}{2}\chi^2 - \alpha_R S\,, \qquad S = \int \rho - m - \rho\,\ln\frac{\rho}{m}$

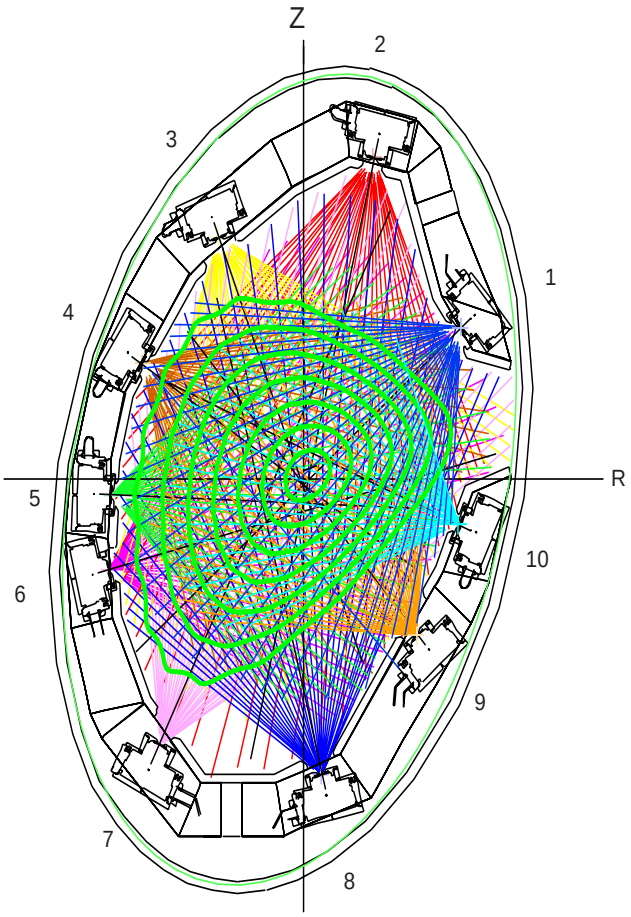

Fig. 1. The10-camera tomographic system on W7-AS, showing the 320 lines of sight that are drawn. Typical $\iota \approx 1/3$ flux surfaces are superimposed. The surrounding ellipse is the W7-AS vessel. The *R*-axis is related to the major radius and the *Z*-axis to the vertical coordinate.

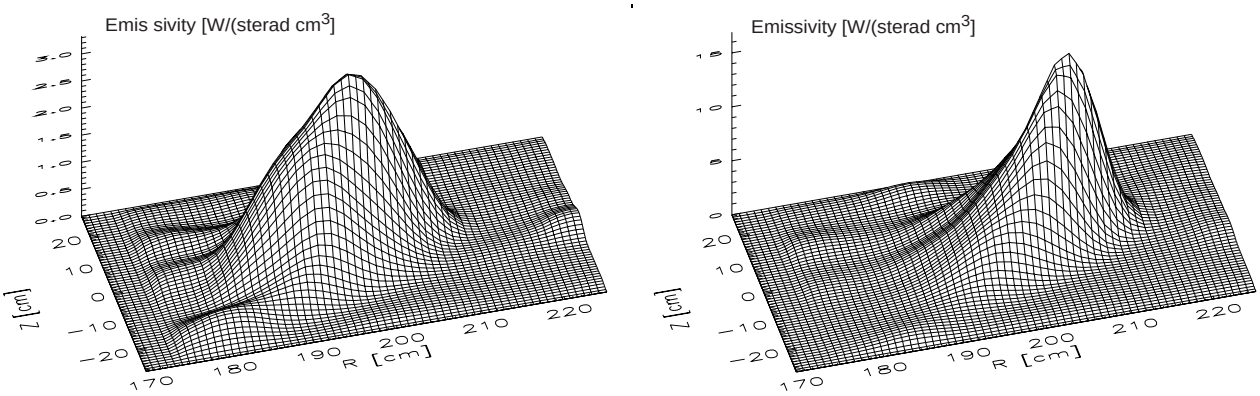

Fig. 2. Equilibrium distribution at different central plasma beta for W7-AS-shot 41618. At left, $\beta_0 \approx 1.3\%$; at right $\beta_0 > 3.8\%$. At high beta, the axis is moved outward by 8 cm; the plasma edge is shifted less, but is not well defined because of the low soft X-ray emission at the plasma edge.

mum of some function Λ that is the sum of the well-known χ^2 -value for a data fit and the product of a regularization parameter α_R and a regularization function R, I_F, S, see Table 1 (ρ is the reconstructed distribution, and m is a default distribution for the maximum entropy reconstruction, which is usually flat).

The regularization parameter controls the relative weighting of reconstructions that fulfill either the data alone or only the minimum of the regularization function. Maximum entropy is not a widely used algorithm, because it requires time-consuming numerical calculations. On the other hand, it is the only algorithm implemented so that the result is a real mathematical result without the need for estimating the regularization parameter. Additionally, error bars for the reconstructed distribution are obtained by this method. Thus, maximum entropy is used for single time equilibrium reconstructions, whereas the faster methods are needed for time series.

For visualization and quantitative analysis, additional processing is necessary. This includes the implementation of different meshes and expansion functions of the emissivity to be reconstructed, singular value decomposition (SVD), filtering in the frequency-space, and error calculations for maximum entropy reconstructions. SVD thereby is the most important method, to extract the fluctuating part of the emissivity attributed to MHD modes from a sequence of reconstructions. In order to check the reliability, simulated plasma radiation distributions were used.

Equilibrium reconstructions

To study equilibrium effects, quantitative measurements of the magnetic surface structure were made. Two effects have been investigated in particular: the change of the plasma shape due to toroidal currents and the effect of the Shafranov shift, which depends on the plasma beta. The reduction of the Shafranov shift is one of the most important optimization criteria of W7-AS. Figure 2 shows a change of about 8 cm in the axis position in an experiment with high plasma beta.

Reconstructions and equilibrium calculations [7] were compared for a mean plasma radius where the soft x-ray profiles have steep gradients, see Fig. 3. For these cases, very good agreement was observed. Only minor differences in the reconstructions were observed in comparing the three tomographic algorithms in Table 1.

MHD activity

We address different kinds of MHD instabilities, including pressure- and current-driven modes and fast particle driven global Alfvén eigenmodes (GAEs). An example is shown in Fig. 4, where different modes are plotted for the case of $m = 3$. The mode type has been identified by knowledge of the driving mechanism. For example, the GAE structures

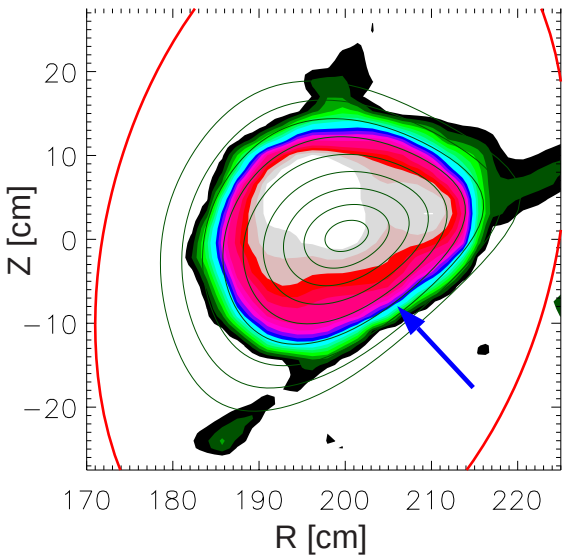

Fig. 3. Equilibrium reconstruction and calculated flux contours. At the radial position, marked with the arrow, steep gradients occur in the soft-X emission and they accurately fix this isoemission line.

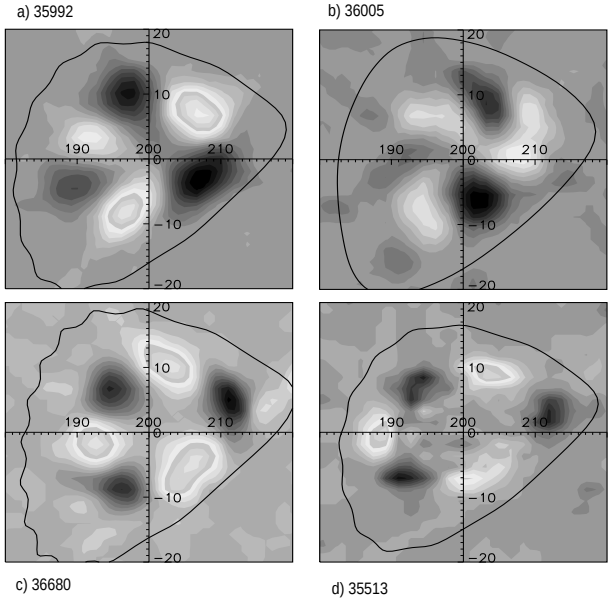

Fig. 4. Four different modes with poloidal mode number m = 3: (a) and (b) GAE; (c) pressure driven mode; (d) tearing mode. The plotted flux surface is at a normalized radius of 0.75.

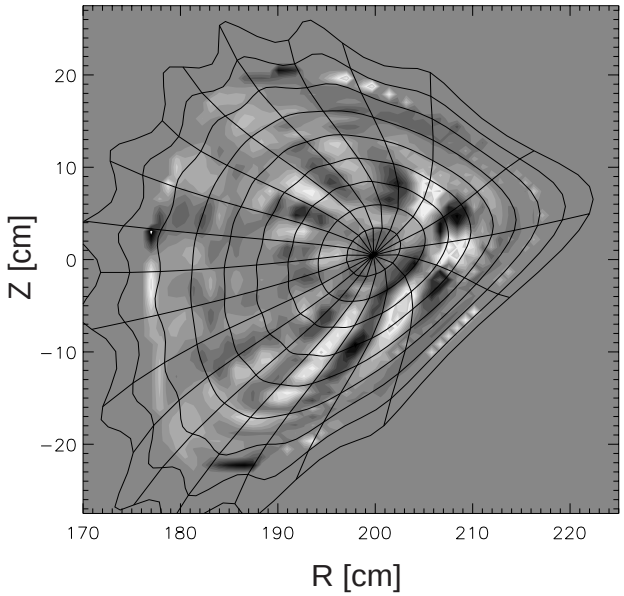

Fig. 5. GAE with m = 9. Here, as basis for the reconstruction space, Fourier-expansion in the magnetic angle is used. The angular phase of the mode agrees with the lines of constant magnetic angle (radial lines).

rotate in the direction given by the ion diamagnetic current, which is opposite to the direction of rotation of the other two mode types. GAEs also extend over a large part of the plasma cross section, but tearing modes and pressure-driven modes are localized around a rational surface [compare, e.g., Fig. 4(a) and Fig. 4(d)].

In the case of GAEs, a variety of peaks found in the Alfvén spectrum were analyzed. Most of the peaks correspond to the lowest (m,n) modes expected from theory (m, n are the poloidal and toroidal mode numbers), but higher m-numbers and modes with different radial structure were also observed. On W7-AS, GAEs are commonly seen with neutral beam heating, and the main features are compatible with theoretical predictions, see Ref. [8]. With the new tomographic system, more complex mode structures can be assessed. For example, Fig. 5 shows an (m = 9) GAE that exists together with an (m = 3) mode and an (m = 6) mode (not plotted). Another W7-AS discharge shows two (m = 3) GAEs: one with a radial node at about R_{eff} = 10 cm (see

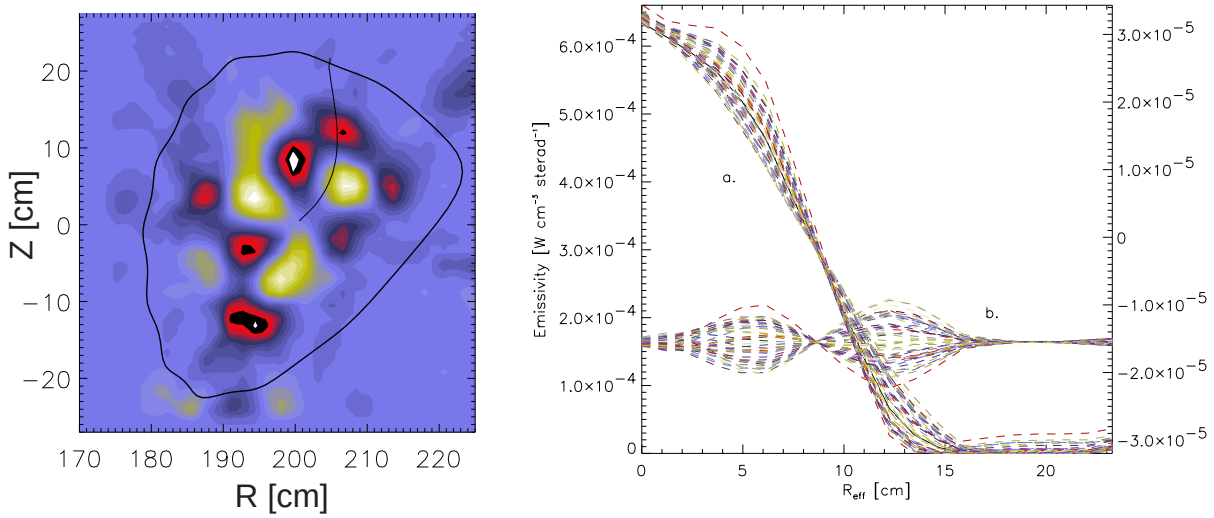

Fig. 6. Radial mode structure found in shot #35982. Left: SVD-filtered picture of the fluctuating emissivity. The radial solid line corresponds to a magnetic angle of $\theta = 40^{o}$. Right: Profiles of the total emissivity profile (a, left axis) and the fluctuations (b, right axis) at different time points (at $\theta = 40^{o}$). For the total profile, the fluctuations are magnified by a factor of 10.

Fig. 6) and the second, without a node (not shown), are observed simultaneously.

In both of these discharges, characterized by $m = \{3, 6, 9\}$ or $m = \{3, 3 \text{ with radial node}\}$. the modes propagate at different frequencies that seem to develop independently during the lifetime of the modes.

C. Görner, M. Anton, J. Geiger, W. von der Linden, A. Weller, S. Zoletnik,❖ W7AS-Team
Max-Planck-Institut für Plasmaphysik
EURATOM Association, D-85748 Garching, Germany
❖KFKI-Research Institute, Department of Plasma Physics
P.O. Box 49, Budapest-114, Hungary

References

[1] R. S. Granetz and P. Smeulders, X-ray tomography on JET, *Nucl. Fusion* **28,** 457 (1988).

[2] G. Grieger et al., "Physics optimization of stellarators," *Phys. Fluids B* **4**(7), 2081 (1992).

[3] S. Zoletnik and S. Kálvin, "A method for tomography using arbitrary expansions," *Rev. Sci. Instrum.* **64**, 1208 (1993).

[4] M. Anton et al., "X-ray tomography on the TVC tokamak," *Plasma Phys. of Controlled Fusion* **38,** 1849 (1996).

[5] W. von der Linden, "Maximum-entropy data analysis," *Appl. Phys. A* **60**, 155 (1994).

[6] K. Ertl et al., "Maximum entropy based reconstruction of soft X-ray emissivity profiles in W7-AS," *Nucl. Fusion* **36**(11), 1477 (1996).

[7] J. Geiger et al., "Review of 3-D equilibrium calculations for W7-AS," *Stellarator News*, No. 53, 3 (1997).

[8] A. Weller et al., "Neutral beam driven global Alfvén eigenmodes in the Wendelstein W7-AS stellarator," *Phys. Rev. Lett.* **72**, 1220 (1994).

LHD central control system focusing on first plasma operation

The present mission of the Large Helical Device (LHD) project is to produce a first plasma as quickly and reliably as possible. In support of this purpose, construction of the Central Operation and Control System (COCOS) began in April 1996 based on the following design philosophies:

1. flexibility for the physics experiment,
2. reliability for the large engineering machine, and
3. extensibility for the central control system.

The first design philosophy requires a user-friendly human-machine interface and advanced real-time plasma control systems; the second requires hard-wired reliable protective interlock systems; and the third leads to distributed and modularized control/monitoring systems.

At the beginning of the LHD proposal process (about 10 years ago), the control system was assumed to be based on a centralized control "process computer." About 5 years later, a Unix engineering workstation system with a VME computer connected by Ethernet LAN was proposed. Now, some client-server systems running Windows NT® have been added for control and data acquisition. These various systems are presently connected by an advanced FDDI/ATM switching network system.

Designed on the basis of the LHD operation scenarios, the control system is composed of the COCOS central unit and several tens of subsupervisory facilities connected by a hard-wired interlock and soft sequential control link in addition to the FDDI/ATM communication network.

More specifically, the COCOS comprises the central control unit (central operation console, central sequence control board, central control computer, central supervision panel, large-scale display, and the VME timing board), the torus instrumentation unit (torus supervision computer, torus supervision VME board, and protective interlock board), the LHD Man-Machine System (LMS), the control data monitoring system, the LHD experimental LAN, and the uninterruptable power supply (UPS) systems. This system is provided with a variety of computers such as Unix engineering workstations, Windows-NT personal computers, VME computer boards with real-time OS (VxWorks), and programmable logic controllers (PLCs).

Figure 1 is a schematic of this system architecture. The central control board with PLCs directly connected to subsystems via hard wiring will be used for the quick and reliable operation of LHD. COCOS supports the reliable protective interlock system. The fast timing system with 64-channel optical signals (accuracy < 1 μs, interval setta-

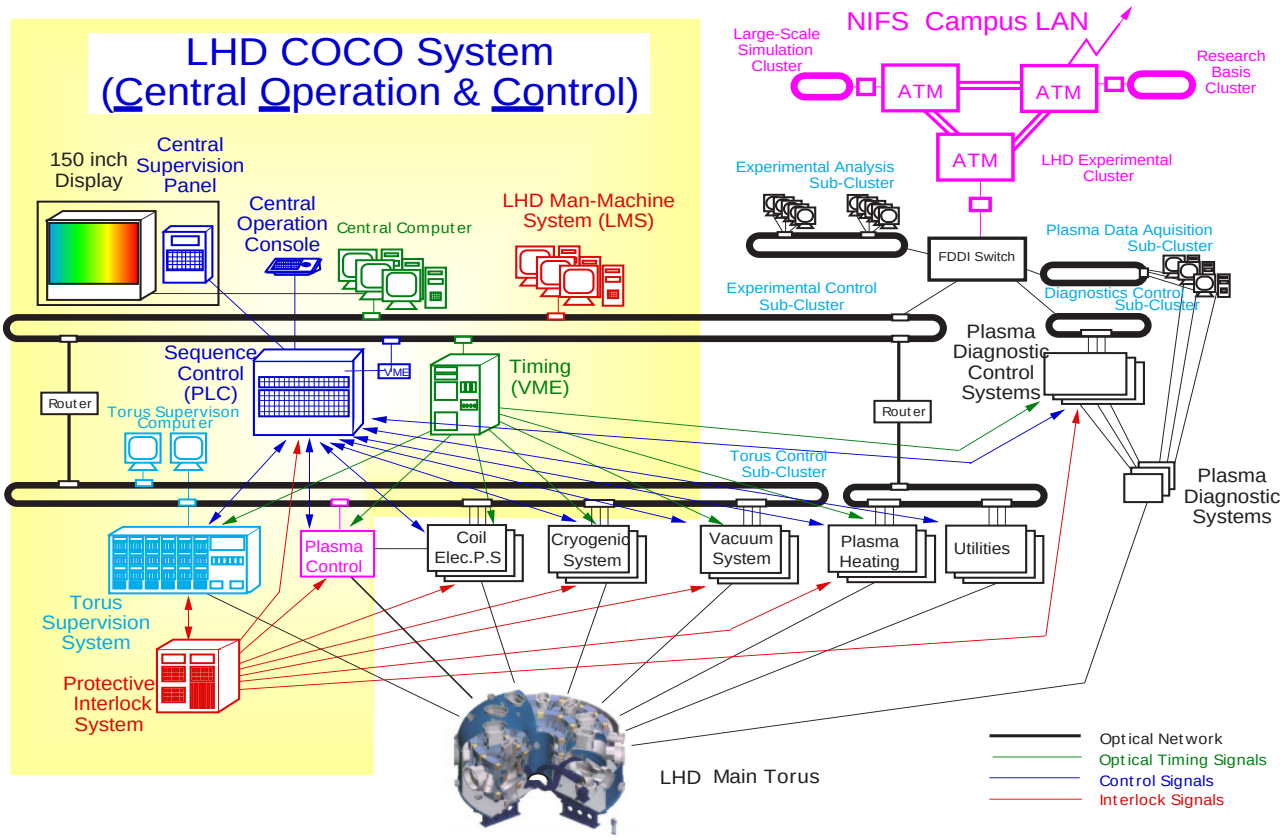

Fig. 1. Schematic of the LHD central operation and control system

ble from 1 ms to 10 h) will be distributed to subsystems. Feedback control for plasma current, position, and cross-sectional shape will be initiated in the near future using intelligent VME control systems, such as applications of fuzzy logic or neural networks in addition to the standard PID plasma control algorithm. For machine supervision, the central data monitoring system is based on Windows NT using a ~1300-channel VME system. The LHD fast data monitoring system with 512-channel VME and the Unix workstation has also been constructed. Full Java computer software on a WWW browser was used in the latter system and will be extended to 4000 channels in the future. To manage experimental data, a relational database was used in this system. The plasma data acquisition system using conventional CAMAC modules is now under construction based on Windows NT. A large supercomputer system for theoretical plasma analyses using the experimental data is connected to the LHD experimental computer by an interlaboratory ATM-LAN system.

At our new site (Toki-city, Gifu-prefecture), the construction of the main experimental hall of the LHD Building was finished in August 1995, and the LHD Control Building with the central control room (Fig. 2) was completed in November 1996. The central control system and the data acquisition client computers were installed in November 1997. The plasma experiment will be started soon (our target is the end of March in 1998), and a variety of experiments will be performed on the LHD device using the flexible and reliable COCOS equipment.

Kozo Yamazaki for the LHD team
Department of Large Helical Device Project
National Institute for Fusion Science
Toki, Japan

E-mail: yamazaki@nifs.ac.jp

Fig. 2. The LHD central control room.

LHD diagnostics

The LHD diagnostics include both many of the standard diagnostics used in previous plasma confinement experiments and ambitious new diagnostics that have been the focus of extensive research and development (R&D).

Table 1 shows a list of diagnostics on LHD. Because we have had eight years of preparations for LHD diagnostics, we have been able to conduct R&D for diagnostics development on both the Japan Institute for Plasma Physics (JIPP) T-IIU tokamak and the Compact Helical System (CHS).

The characteristics of the LHD diagnostics may be summarized in the following two ways.

First, detailed radial profiles of various physical quantities are measured by devices such as a 200-spatial-point YAG

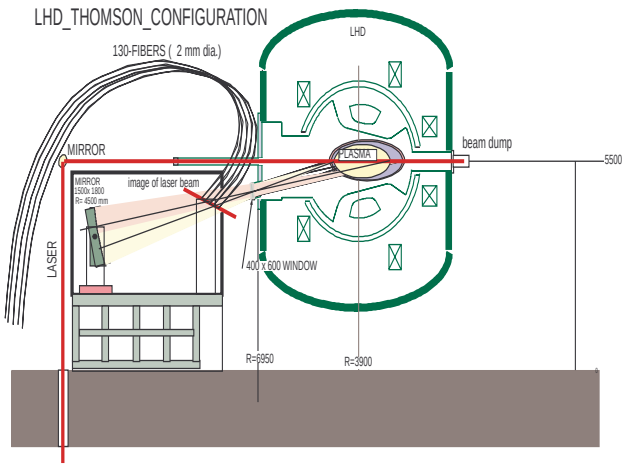

Fig. 1. Schematic of the 200-spatial point YAG Thomson scattering system for LHD.

Table 1. LHD Diagnostics

Diagnostic	Purpose	Brief Description
Magnetic probes	I_p, P_{pl}, position and shape of plasma	Rogowski, Mirnov, flux loops
Microwave interferometer	$n_e L$	2-mm/1-mm wave, single channel
FIR laser interferometer	$n_e L(r)$	119-mm CH_3OH laser, 10 channels
Microwave reflectometer	n_e, n_e fluctuation	Under development
Thomson scattering	$T_e(r)$, $n_e(r)$	200 spatial points
ECE	$T_e(r, z)$	2-D imaging
X-ray pulse height spectrometer	T_e, Impurities	20-channel Si(Li), 4-channel Ge detector
NPA	T_i, $f(E)$	Radial scan
CXRS	$T_i(r)$, $V_p(r)$	Uses diagnostic neutral beam
X-ray crystal spectrometer	$T_i(r)$	0.1–4 nm, $\lambda/\Delta\lambda$: 10^4
Neutron diagnostics	neutron flux, T_i	NE-213 detectors, ^{3}He counters, activation of metal foils
Bolometers	$P_{rad}(r)$	Metal film, silicon diode, pyrolytic
VUV spectroscopy	Impurities, T_i	1–200 nm, $\lambda/\Delta\lambda$: 10^4
Visible spectroscopy	n_0(H), Z_{eff}	200–700 nm, $\lambda/\Delta\lambda$: 5 x 10^4
Langmuir probes	T_e, n_e	Fast scanning and fixed probes
Visible/infrared TV	Plasma position, plasma wall interactions, wall/limiter temperature	TV system
Soft X-ray diode array	MHD oscillations	Silicon surface-barrier diodes
Microwave/FIR laser scattering	Microinstabilities	1-mm/195-mm multichannel
Heavy ion beam probe	Φ_p, Φ_p fluctuation	Au^- or Tl^+, 6 MeV, 100 mA
Diagnostic pellet	Particle transport	Hydrogen/DL ice pellet, C, Li
High-energy particle diagnostics	High-energy particles	Li / He beam (2 MeV, 10 mA) probe, particle detector probes

Thomson scattering apparatus (Fig. 1, designed and prepared by K. Narihara et al.) and a 13-channel FIR interferometer, a fast-scan 3-m VUV spectrometer and charge-exchange recombination spectroscopy (CXRS) for ion temperature profiles, and a two-dimensional bolometer array.

Second, the plasma potential is directly measured by a heavy ion beam probe (HIBP) (Fig. 2, designed and prepared by H. Iguchi et al.). The required energy of the beam is 6 MeV for 3-T operation of LHD. We used the 8-year preparation period to construct and operate a 0.5-MeV HIBP on JIPP T-IIU and a 0.2-MeV HIBP on CHS. This enabled us to design the system and to get actual experience with high-voltage engineering and ion sources.

We will also measure the density turbulence in order to understand the causes of anomalous transport. The development of the reflectometer has been performed as a preparation activity at JIPP T-IIU and CHS. The 6-MeV HIBP may also be a potential tool for turbulence study if the beam diameter can be small. Since millimeter-wave scattering will be helpful for the study of LHD plasma turbulence, we want to construct such a system in the early future.

Yasuji Hamada for the LHD team
National Institute for Fusion Science
Toki, Japan
E-mail: hamada@nifs.ac.jp

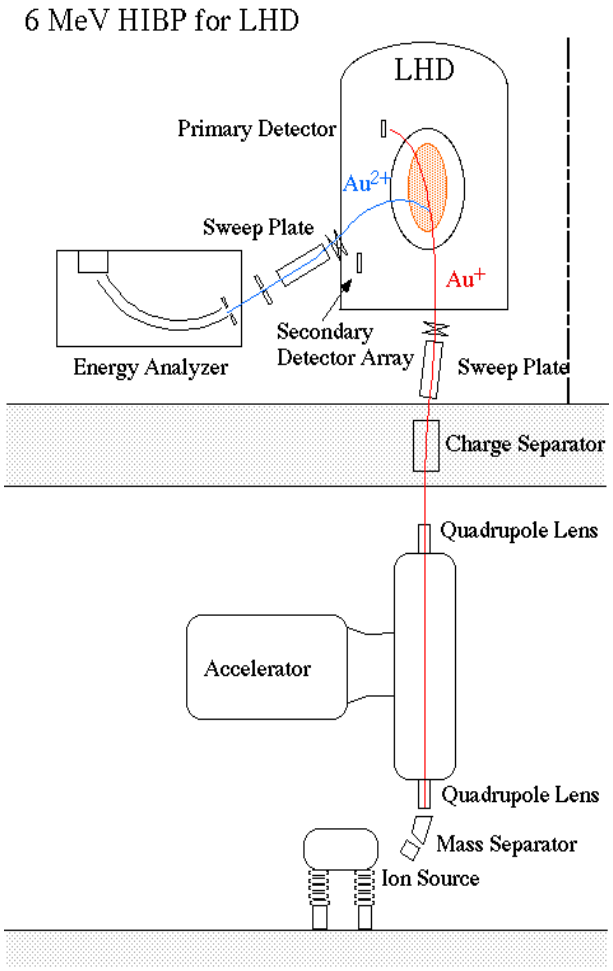

Fig. 2. The LHD 6-MeV heavy ion beam probe.